flux amplifier or transducer. Figure 5b illustrates how the pump can be used to demagnetize a sample[15]. The left-hand frame shows the flux trapped in our sample after the application and subsequent removal of $H_c = 4$ Oe at 85 K ($H_{//} = 0$). An in-plane field, $H_{//} = 35$ Oe, was then applied, driving the sample into the vortex chain state (middle frame). Finally, the in-plane field $H_{//}$ was slowly removed and, as the JVs were swept out of the sample they dragged the PVs with them, leaving a demagnetized sample (right-hand frame).

Magnetic irreversibility in layered superconductors is known to be suppressed by the application of either a.c.[6,15] or d.c. in-plane magnetic fields. The movie images shown in Fig. 5c yield insights into the latter situation, where H_c has been increased from 2 Oe at fixed $H_{//} = 35$ Oe at 81 K. We find that PVs preferentially penetrate along the 1D vortex chains (left hand and middle frames), and only propagate into the inter-chain spaces if the chain density becomes saturated (right-hand frame) as explained in Fig. 2 legend. It seems that the PV stack structure induced by the JV currents weakens the interaction with quenched sample disorder, and the mobility of PVs along the 1D chains is considerably higher than in the inter-chain spaces. Magnetization loops measured with the scanning Hall probe retracted from the sample surface confirm this conclusion, and reveal a marked suppression of the irreversibility in the presence of JVs ($H_{//} \neq 0$). PV penetration in this regime is known to be limited by electromagnetic surface barriers[16], which will be slightly lower where JVs intercept the edges, owing to the superposition of Meissner and JV currents. Hence PVs preferentially enter at the sample edges along JVs where surface barriers are lowest, and then show a much higher mobility along the 1D vortex chains. □

Received 2 May; accepted 19 October 2001.

1. Kleiner, W. H., Roth, L. M. & Autler, S. H. Bulk solution of Ginzburg-Landau equations for type II superconductors: upper critical field region. *Phys. Rev. A* **133,** 1226–1227 (1964).
2. Clem, J. R. Anisotropy and two-dimensional behaviour in the high-temperature superconductors. *Supercond. Sci. Technol.* **11,** 909–914 (1998).
3. Bulaevski, L. N., Levdij, M. & Kogan, V. G. Vortices in layered superconductors with Josephson coupling. *Phys. Rev. B* **46,** 366–380 (1992).
4. Huse, D. A. Magnetic-flux patterns on the surface of a type-II superconductor. *Phys. Rev. B* **46,** 8621–8623 (1992).
5. Koshelev, A. E. Crossing lattices, vortex chains, and angular dependence of melting line in layered superconductors. *Phys. Rev. Lett.* **83,** 187–190 (1999).
6. Farrell, D. E. *et al.* Magnetization jumps and irreversibility in $Bi_2Sr_2CaCu_2O_8$. *Phys. Rev. B* **53,** 11807–11816 (1996).
7. Bolle, C. A. *et al.* Observation of a commensurate array of flux chains in tilted flux lattice in Bi-Sr-Ca-Cu-O single crystals. *Phys. Rev. Lett.* **66,** 112–115 (1991).
8. Grigorieva, I. V., Steeds, J. W., Balakrishnan, G. & Paul, D. M. Vortex-chain state in $Bi_2Sr_2CaCu_2O_{8+\delta}$—experimental evidence for coexistence of 2 vortex orientations. *Phys. Rev. B* **51,** 3765–3771 (1995).
9. Oral, A., Bending, S. J. & Henini, M. Real-time scanning Hall probe microscopy. *Appl. Phys. Lett.* **69,** 1324–1326 (1996).
10. Grier, D. G. *et al.* Translational and bond-orientational order in the vortex lattice of the high-T superconductor $Bi_{2.1}Sr_{1.9}CaCu_2O_{8+x}$. *Phys. Rev. Lett.* **66,** 2270–2273 (1991).
11. Martinez, J. C. *et al.* Magnetic anisotropy of a $Bi_2Sr_2CaCu_2O_x$ single crystal. *Phys. Rev. Lett.* **69,** 2276–2279 (1992).
12. Zeldov, E. *et al.* Thermodynamic observation of first-order vortex-lattice melting transition in $Bi_2Sr_2CaCu_2O_8$. *Nature* **375,** 373–376 (1995).
13. Soibel, A. *et al.* Imaging the vortex-lattice melting process in the presence of disorder. *Nature* **406,** 282–287 (2000).
14. Nelson, D. R. Vortex entanglement in high-T_c superconductors. *Phys. Rev. Lett.* **60,** 1973–1976 (1988).
15. Avraham, N. *et al.* Inverse melting of a vortex lattice. *Nature* **411,** 451–454 (2001).
16. Burlachkov, L. *et al.* Giant flux-creep through surface barriers and the irreversibility line in high temperature superconductors. *Phys. Rev. B* **50,** 16770–16773 (1994).

Acknowledgements

We thank M.J.W. Dodgson for discussions. This work was supported in the UK by the EPSRC and the MOD, in the USA by MARTECH, Florida State University, and in Japan by the Ministry of Education, Science, Sports and Culture.

Competing interests statement

The authors declare that they have no competing financial interests.

Correspondence and requests for materials should be addressed to S.B. (e-mail: pyssb@bath.ac.uk).

High-temperature ultrafast polariton parametric amplification in semiconductor microcavities

M. Saba*, C. Ciuti*, J. Bloch†, V. Thierry-Mieg†, R. André‡, Le Si Dang‡, S. Kundermann*, A. Mura§, G. Bongiovanni§, J. L. Staehli* & B. Deveaud*

* *Physics Department, Swiss Federal Institute of Technology Lausanne, PH-Ecublens, CH-1015 Lausanne-EPFL, Switzerland*
† *Centre National de la Recherche Scientifique, L2M-CNRS, 92225 Bagneux Cedex, France*
‡ *Laboratoire de Spectrometrie Physique, Université J. Fourier-Grenoble, F-38402 Saint Martin d'Hères Cedex, France*
§ *Dipartimento di Fisica and Istituto Nazionale di Fisica della Materia, Università degli Studi di Cagliari, I-09042 Monserrato, Italy*

Cavity polaritons, the elementary optical excitations of semiconductor microcavities, may be understood as a superposition of excitons and cavity photons[1]. Owing to their composite nature, these bosonic particles have a distinct optical response, at the same time very fast and highly nonlinear. Very efficient light amplification due to polariton–polariton parametric scattering has recently been reported in semiconductor microcavities at liquid-helium temperatures[2–11]. Here we demonstrate polariton parametric amplification up to 120 K in GaAlAs-based microcavities and up to 220 K in CdTe-based microcavities. We show that the cut-off temperature for the amplification is ultimately determined by the binding energy of the exciton. A 5-μm-thick planar microcavity can amplify a weak light pulse more than 5,000 times. The effective gain coefficient of an equivalent homogeneous medium would be 10^7 cm^{-1}. The subpicosecond duration and high efficiency of the amplification could be exploited for high-repetition all-optical microscopic switches and amplifiers. 10^5 polaritons occupy the same quantum state during the amplification, realizing a dynamical condensate of strongly interacting bosons which can be studied at high temperature.

A semiconductor microcavity is a photonic structure designed to enhance light–matter interaction. The cavity photons are confined between two mirrors, and resonantly interact with the excitonic transition of a two-dimensional semiconductor quantum well (Fig. 1). In the strong-coupling regime, the normal modes of the system are the cavity polaritons, which are half-exciton, half-photon quasiparticles[1]. The energies of the two polariton modes anticross when the energy difference between exciton and photon modes is varied (Fig. 1). The minimum polariton splitting measures the strength of the coupling. Owing to their excitonic content, polaritons are subject to Coulomb interaction and give rise to strong optical nonlinearities. At the same time, owing to the photon component, the curve of polariton energy dispersion versus in-plane wavevector is very steep, meaning that it is quite sensitive to the excitation angle (Fig. 1). A small number of states can be excited at a given angle, and quantum degeneracy (more than one polariton per state) is achieved with relatively low excitation densities. The bosonic statistics strongly enhances some particular scattering processes, provided that the density is kept below the critical value where the bosonic behaviour of excitons breaks down owing to the appearance of the fermionic nature of electrons and holes, which make up the excitons[12]. The scattering from an incoherent exciton reservoir into polaritons can be stimulated by the occupation of the final state[13] and give rise to a polariton laser[14]. If, as in our case, coherent polaritons are injected into the cavity, the phase-coherent final-state stimulation (termed parametric amplification) can be much more efficient than in the incoherent case[2–11].

© 2001 Macmillan Magazines Ltd

To investigate the coherent regime, polaritons are resonantly excited by a pump laser pulse on the lower-polariton dispersion curve[2] (Fig. 1). The excitation angle is chosen to allow energy and momentum conservation for the scattering between two polaritons, one into the lowest-energy state (with in-plane wavevector $k = 0$) and the other into a higher-energy state ($2E_k = E_0 + E_{2k}$ has to be fulfilled, where E_k is the energy of a pump polariton injected with an in-plane wavevector k). A weak probe beam (the 'signal'), injected perpendicular to the cavity ($\theta = 0$), stimulates the scattering into the lowest-energy state at the bottom of the dispersion curve ($k = 0$). This non-degenerate wave-mixing process can also be seen as optical parametric amplification. The exciton content makes the polariton–polariton interaction very efficient[5], and gains of up to 100 on the probe beam have been reported at liquid-helium temperatures[2]. The spontaneous relaxation of a few pump polaritons into the lowest-energy state can also trigger parametric scattering under continuous-wave optical pumping and without an external probe[7–11]. In order to exploit this nonlinear phenomenon in practical devices, one of the challenges is to demonstrate the polariton parametric process at high temperatures.

We show here that engineering the sample structure in order to maximize the exciton–photon coupling greatly increases the parametric polariton amplification, giving optical gains up to 5,000. The amplification survives at high temperatures, up to 220 K in the CdTe microcavity, approaching room temperature and allowing the design of several possible devices. We find that in the structures we considered, the cut-off temperature of the parametric gain scales linearly with the binding energy of the exciton.

The polariton splitting in microcavities is proportional to the square root of the oscillator strength of the excitonic transition, and can be increased by inserting a large number of quantum wells into the cavity. Here we consider GaAlAs-based and CdTe-based microcavities grown by molecular-beam epitaxy. The 3λ CdTe-based cavity contains six stacks of four quantum wells, at the antinodes of the electric field, giving a 25-meV low-temperature polariton splitting. In the GaAlAs-based microcavities, a few quantum-well stacks are also placed in the dielectric mirrors (distributed Bragg reflectors), at positions corresponding to the maxima of light intensity[15] (Fig. 1). With this arrangement, the exciton also couples to the light field penetrating the mirrors, giving large polariton splittings—15.3 meV (12 quantum wells) and 20 meV (36 wells)—in spite of the lower excitonic oscillator strength of the GaAlAs-based structures compared to CdTe-based structures. In all three samples, the polariton anticrossing is observed up to room temperature.

The pump–probe measurements presented here are taken in reflection geometry: the sample is illuminated by transform-limited 250-fs-long pulses from a mode-locked Ti:sapphire laser with an 80-MHz repetition rate. A mechanical goniometer allows us to vary the pump angle while keeping constant the pump–probe delay; the weak probe beam hits the sample nearly at normal incidence. To avoid a non-uniform excitation, the centre of the probe spot on the sample is spatially selected by a pin-hole.

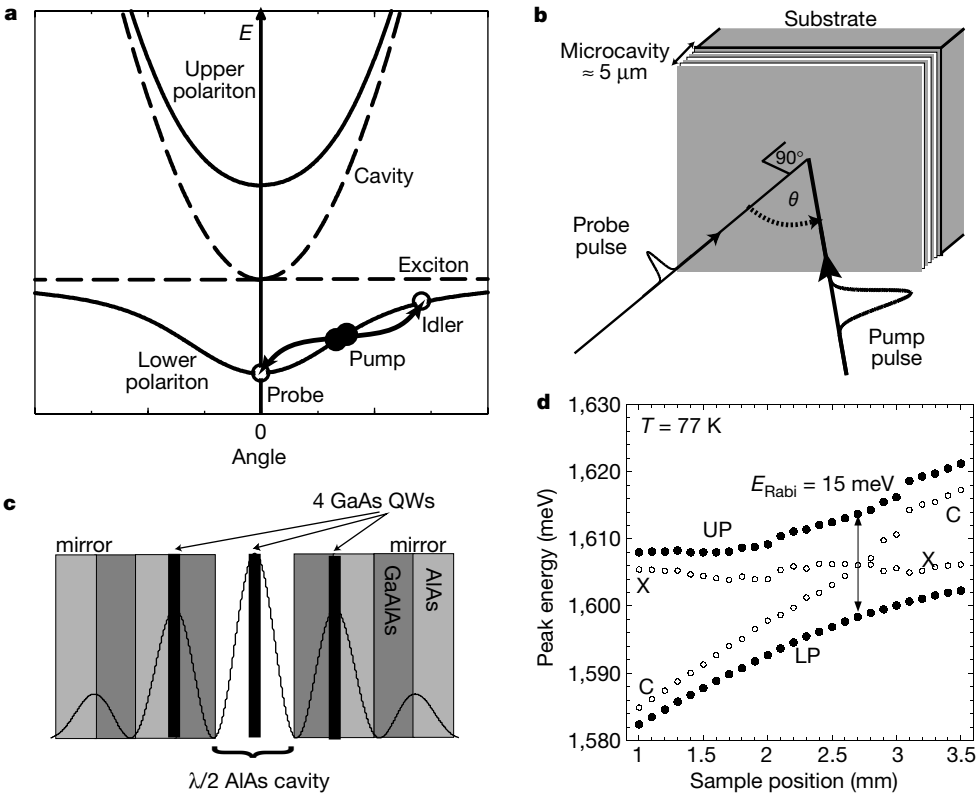

Figure 1 Principle of the pump–probe optical set-up and sample characteristics. **a**, Sketch of the polariton energy E versus the incidence angle θ of the exciting light. The corresponding in-plane wavevector k of the excited polariton is given by $k = (\omega/c)\sin\theta$, where ω is the light frequency. The parametric polariton–polariton scattering process is also depicted. **b**, Angle-resolved pump–probe configuration. **c**, GaAlAs-based sample structure, with three stacks of four quantum wells (QWs). The 7-nm-wide GaAs wells are separated by 3-nm-wide AlAs barriers. The Bragg mirrors consist of alternating $Ga_{0.8}Al_{0.2}As$/AlAs λ/4 layers. The solid line depicts the qualitative behaviour of the electric field intensity in the cavity. Another sample was prepared with nine stacks of wells[14] (36 wells). In the CdTe-based sample, six stacks of four wells each are placed at the six antinodes of the electric field inside a 3λ cavity. The 24 5-nm-wide CdTe wells are separated by 6-nm-wide $CdMg_{0.6}Te$ barriers. Alternating λ/4 layers of $CdMg_{0.6}Te$ and $CdMn_{0.25}Te$ act as cavity mirrors. **d**, The cavities are wedge-shaped, so that by varying the position on the sample the cavity energy also varies. By tuning the cavity energy (G) with respect to the excitonic energy (*X*, which is instead almost constant), the anticrossing of the polariton energies is observed. The polariton energies (filled circles) for the GaAlAs sample are measured from the linear reflectivity spectra, while the exciton and the cavity energies (open circles) are extracted from the data with a two coupled oscillators model. LP, lower-polariton energy; UP, upper-polariton energy; E_{Rabi}, minimum polariton splitting.

© 2001 Macmillan Magazines Ltd

The probe beam is greatly amplified (Fig. 2)—by a factor of up to 5,000 in one of our GaAlAs-based samples, a gain nearly two orders of magnitude higher than in previous reports[2]. The strong line appearing in the gain spectra is narrower than the lower polariton, and lies between the energy of the unperturbed polariton and that of the cavity mode. Because the interaction between co-polarized polaritons (through their excitonic components) turns out to be repulsive, the whole polariton branch is shifted towards higher energies, and the gain spectrum peaks on the high-energy tail of the unperturbed polariton absorption line[5]. The maximum gain occurs at the angle corresponding to the inflection point of the dispersion curve of the lower polariton, where the energy and momentum conservation for the parametric scattering is most easily satisfied. The width of the angular resonance depends on the broadness of the energy distribution of pump polaritons, and is therefore related to the polariton spectral linewidth. The curve of gain versus pump power shows a sharp threshold, typical of stimulated scattering. Close to threshold, the probe gain can be increased by a factor of 10 by increasing the pump power by less than 50%, a highly desirable feature for an optical switch device.

Using the parameters of the experiment, we calculate that each probe pulse populates each state with approximately 100 polaritons (details on how to count the available polariton states are given in ref. 8). The parameters used for this estimate are the probe-beam angle spread (0.5°) and the probe photon density injected into the cavity (2×10^6 photons per cm^2 per pulse). When the gain is 5,000, the light intensity emitted in the probe direction after the parametric amplification is 2,500 times that absorbed from the probe: this is because the gain peak is approximately twice as narrow as the polariton. The resulting occupancy of the lowest-energy state is of the order of 10^5 polaritons per state. Even taking only 20% of the exciton fraction for each polariton, more than 10,000 excitons are in the same state. The device thickness along the growth direction is about 5 μm, so the amplification would correspond, if directly expressed as an effective material gain, to an impressive coefficient of $10^7\ cm^{-1}$.

The parametric gain in the cavities featuring large polariton splittings is robust enough to survive up to 125 K in the GaAlAs samples and up to 220 K in the CdTe sample (Fig. 3). We note that

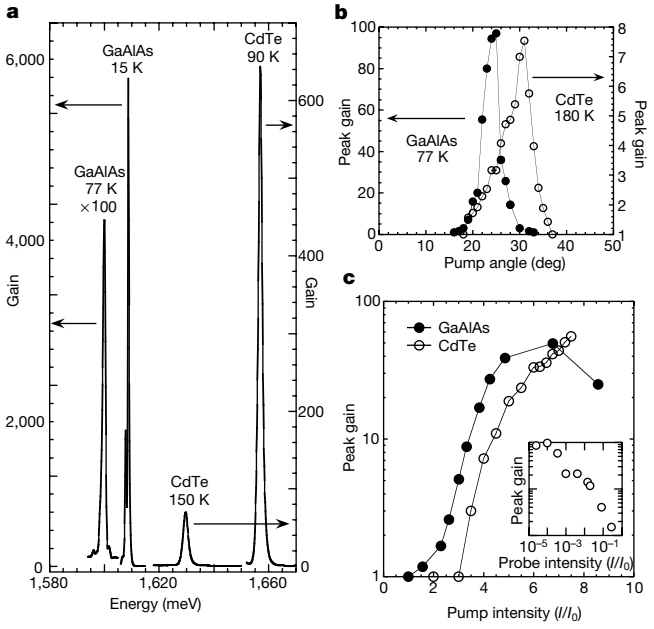

Figure 2 Main features of parametric gain: high efficiency, spectrally narrow lines, angular resonance and pump-power threshold. **a**, Gain spectra for different temperatures in the GaAlAs-based (12 wells) and CdTe-based samples. When the temperature increases, the polariton mode gets broader because of the thermal dephasing and consequently the gain peak gets smoother, broader and less intense. The energy of the polariton, and consequently that of the parametric gain, varies with temperature, as it follows the bandgap thermal redshift. The maximum gain occurs when the cavity mode energy is lower than the exciton energy by about half the polariton splitting. **b**, Angular resonance: in the CdTe sample, the maximum gain occurs at a higher angle than in the GaAlAs sample (the polariton splitting is larger) and the angular resonance is broader owing to the broader polariton line. **c**, The power dependence of peak gain (the highest value extracted from the spectra at the resonance angle) shows a threshold and then saturates at high powers. $I_0 = 10^{13}$ photons per cm^2 per pulse. The temperature is 77 K for the GaAlAs sample, 150 K for the CdTe sample. The threshold is reached at lower fluences in the GaAlAs sample owing to the lower number of wells inside the cavity and the smaller excitonic oscillator strength. Inset, the gain (normalized to its maximum value) is reduced by raising probe power (data are for the CdTe sample at $T = 90$ K; for other samples and temperatures, similar behaviour is found).

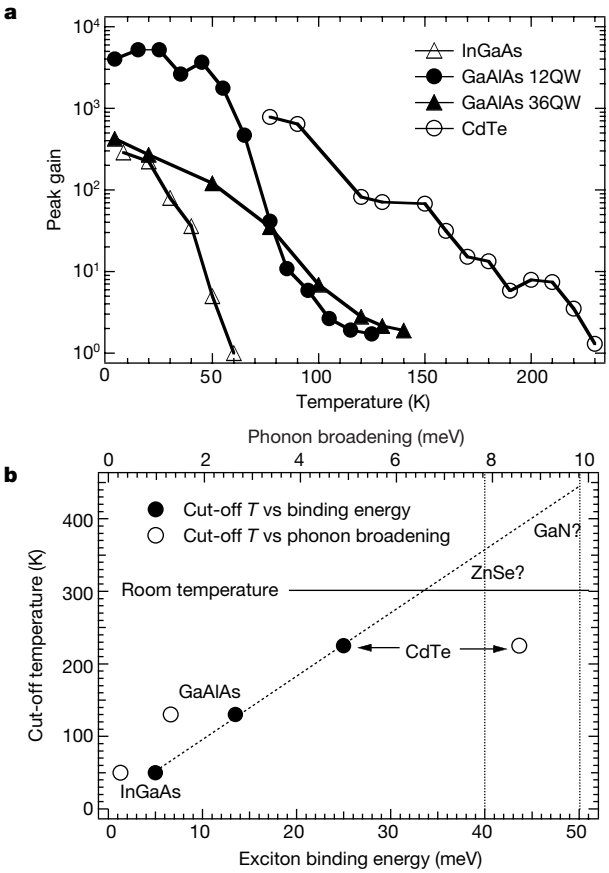

Figure 3 Temperature dependence of parametric gain. **a**, Peak gain versus temperature for the different samples. The CdTe cavity is designed to match the exciton energy at high temperatures; below 77 K, exciton–photon resonance is no longer achieved. The measurements are taken for the same pump fluence for both GaAlAs samples, but owing to the greater threshold for the 36-well sample, at low temperatures the gain is lower than in the 12-well sample (the pump fluence needed to saturate the gain in the 36-well sample could not be achieved with our laser). **b**, Cut-off temperatures for the gain in different materials as a function of the exciton binding energy (lower *x* axis, filled circles). The broken line is a linear fit to the data. The inverse logarithmic slope of the last points on each curve has the same dependence on the binding energy. The vertical dotted lines mark the typical exciton binding energies in ZnSe- and GaN-based quantum wells. In contrast, the cut-off temperature seems not to scale with the line broadening owing to the exciton–phonon coupling (upper *x* axis, open circles). The phonon broadening at the cut-off temperature is the product of the number of phonons in the lattice (determined only by the temperature and the phonon energy, 36 meV in GaAs, 21 meV in CdTe) times the exciton–phonon coupling coefficient (13.8 meV in GaAs, 15 meV in CdTe).

© 2001 Macmillan Magazines Ltd

the gains of the two GaAlAs samples (one with 12 wells, and one with 36) show a very similar cut-off temperature, although the two samples have different polariton splittings. (The cut-off temperature is defined as the temperature at which the gain falls to 1, the highest possible operation temperature for the device.) This feature indicates that beyond a certain point the cut-off temperature does not rise any more with the polariton splitting, and is limited by some intrinsic parameter of the material. The CdTe sample, having a polariton splitting only 25% larger than that of the GaAlAs samples, sustains the parametric amplification up to almost twice the temperature. What is very different in the two materials is the exciton binding energy—that is, the energy separating the quasi-bosonic bound exciton states from the fermionic continuum of unbound electron–hole pairs. In the 7-nm-wide GaAs quantum wells, the exciton binding energy is about 13.5 meV, whereas in the CdTe wells it is about 25 meV. As a check of the binding-energy dependence, we repeated the experiment on an InGaAs-based microcavity with a 5-meV exciton binding energy, and found that it only shows gain up to 50 K. The dependence of the cut-off temperature on the exciton binding energy appears to be linear. This indicates that the cut-off temperature is related to the dissociation of polaritons or excitons into free carriers. In the linear regime this process does not significantly alter the optical response, as the polariton peaks are still well resolved at the cut-off temperature and the polariton splitting is reduced by only 10% with respect to the low-temperature value. The presence of fermionic free carriers has instead a marked effect on the nonlinear regime, as the parametric amplification critically depends on a limitation on the occupancy per state and on the degree of coherence of the polaritons[5].

We note that the cut-off temperature scales linearly with the exciton binding energy in GaAs and CdTe microcavities, whereas it does not seem to depend on the phonon parameters (Fig. 3). The optical phonon energy and the matrix element of the exciton–phonon interaction strongly depend on the material parameters, and are expected to contribute to the efficiency of thermal dissociation of polaritons. Further investigations of other structures with larger exciton binding energies will help to understand the exact effect of the exciton–phonon interaction on the parametric gain. Suitable materials for such studies are some II–VI compounds, such as ZnSe, which have exciton binding energies as high as 40 meV (ref. 16). Furthermore, the exciton binding energy (in sufficiently narrow wells) can be made larger than the optical phonon energy (as in CdTe), thus greatly suppressing the thermal ionization process. We expect GaN-based semiconductor compounds to attract attention in the future, owing to their very high oscillator strengths[17,18]. Efforts at present are concentrated on the growth technology of nitride compounds in order to improve the sample quality and achieve strong coupling in microcavities. The strong-coupling regime at room temperature has already been demonstrated in organic microcavities[19,20], with large polariton splittings of around 100 meV. Even if the coherence time of optical excitations in such compounds is very short, the low material costs and simple sample preparation will encourage studies of ultrafast polaritonic nonlinearities.

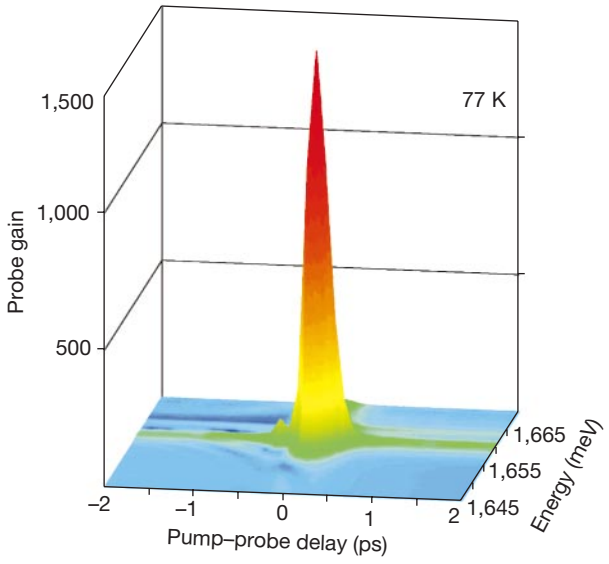

Figure 4 The probe reflectivity spectrum of the CdTe sample as a function of the pump–probe delay, showing the ultrafast dynamics of the parametric gain.

The time dynamics of the parametric amplification can be explored by delaying the probe pulse with respect to the pump. The amplification lasts as long as pump and probe polariton waves are simultaneously inside the cavity, leading to ultrafast dynamics (Fig. 4). Moreover, the polaritons injected by the pump escape from the cavity within a few picoseconds after the excitation, so that a device based on polariton parametric amplification could have a very fast recovery time, with a physical limit for the repetition rate in the terahertz range. Further, because the light of the amplified probe pulse comes from a collective coherent polariton state, control of the polariton wavefunction inside the cavity by means of optical pulses could result in complete and ultrafast control of the amplitude, phase and spectral shape of the emitted light.

The massive occupation of the lowest-energy polariton state can be also seen as a dynamical condensation of polaritons. In comparison to the Bose condensation of atoms, polariton condensation occurs for strongly interacting particles[4], at higher densities (the ratio between the particle spacing and their radius is of the order of 10 for polaritons and about 1,000 for atoms), with a much stronger coupling with the environment (a typical loss rate in microcavities is $10^{12}\ s^{-1}$, compared to $10^{5}\ s^{-1}$ for atomic systems): most notably, polariton condensation occurs at temperatures of the order of 100 K instead of 10^{-8} K. Semiconductor microcavities therefore offer the possibility of studying at 100 K the non-classical states of matter realized in dynamical condensates. □

Received 12 June; accepted 8 October 2001.

1. Weisbuch, C., Nishioka, M., Ishikawa, A. & Arakawa, Y. Observation of the coupled exciton-photon mode splitting in a semiconductor quantum microcavity. *Phys. Rev. Lett.* **69,** 3314–3317 (1992).
2. Savvidis, P. G. *et al.* Angle-resonant stimulated polariton amplifier. *Phys. Rev. Lett.* **84,** 1547–1551 (2000).
3. Ehrenstein, D. Amplifier from half-breed particles. *Phys. Rev. Focus* **5,** story 6 (2000).
4. Yamamoto, Y. Half-matter, half-light amplifier. *Nature* **405,** 629–630 (2000).
5. Ciuti, C., Schwendimann, P., Deveaud, B. & Quattropani, A. Theory of the angle-resonant polariton amplifier. *Phys. Rev. B* **62,** R4825–R4828 (2000).
6. Dasbach, G., Baars, T., Bayer, M., Larionov, A. & Forchel, A. Coherent and incoherent polaritonic gain in a planar semiconductor microcavity. *Phys. Rev. B* **62,** 13076–13083 (2000).
7. Houdré, R., Weisbuch, C., Stanley, R. P., Oesterle, U. & Ilegems, M. Nonlinear emission of semiconductor microcavities in the strong coupling regime. *Phys. Rev. Lett.* **85,** 2793–2796 (2000).
8. Stevenson, R. M. *et al.* Continuous wave observation of massive polariton redistribution by stimulated scattering in semiconductor microcavities. *Phys. Rev. Lett.* **85,** 3680–3683 (2000).
9. Savvidis, P. G. *et al.* Asymmetric angular emission in semiconductor microcavities. *Phys. Rev. B* **62,** R13278–R13281 (2000).
10. Baumberg, J. J. *et al.* Parametric oscillation in a vertical microcavity: a polariton condensate or micro-optical parametric oscillation. *Phys. Rev. B* **62,** R16247–R16250 (2000).
11. Ciuti, C., Schwendimann, P. & Quattropani, A. Parametric luminescence of microcavity polaritons. *Phys. Rev. B* **63,** 041303R-1–041303R-4 (2001).
12. Imamoglu, A., Ram, R. J., Pau, S. & Yamamoto, Y. Nonequilibrium condensates and lasers without inversion: exciton-polariton lasers. *Phys. Rev. A* **53,** 4250–4253 (1996).
13. Huang, R., Tassone, F. & Yamamoto, Y. Experimental evidence of stimulated scattering of excitons into microcavity polaritons. *Phys. Rev. B* **61,** R7854–R7857 (2000).
14. Le Si Dang, Heger, D., André, R., Boeuf, F. & Romestain, R. Stimulation of polariton photoluminescence in semiconductor microcavity. *Phys. Rev. Lett.* **81,** 3920–3923 (1998).
15. Bloch, J., Freixanet, T., Marzin, J. Y., Thierry-Mieg, V. & Planel, R. Giant Rabi splitting in a microcavity containing distributed quantum wells. *Appl. Phys. Lett.* **73,** 1694–1696 (1998).
16. Kelkar, P. V. *et al.* Stimulated emission, gain and coherent oscillations in II-VI semiconductor microcavities. *Phys. Rev. B* **56,** 7564–7573 (1997).
17. Ponce, F. A. & Bour, D. P. Nitride-based semiconductors for blue and green light-emitting devices. *Nature* **386,** 351–359 (1997).
18. Pearton, S. J., Zolper, J. C., Shul, R. J. & Ren, F. GaN: processing, defects, and devices. *J. Appl. Phys.* **86,** 1–78 (1999).

© 2001 Macmillan Magazines Ltd

19. Lidzey, D. G. *et al.* Strong exciton–photon coupling in an organic semiconductor microcavity. *Nature* **395,** 53–56 (1998).
20. Lidzey, D. G., Bradley, D. D. C., Armitage, A., Walker, S. & Skolnick, M. S. Photon-mediated hybridisation of Frenkel excitons in organic semiconductor microcavities. *Science* **288,** 1620–1623 (2000).

Acknowledgements

We thank U. Oesterle and R. Houdré for growing the InGaAs sample, and J.D. Ganiere, G. Hayes, A. Quattropani, R. Romestain, P. Senellart and P. Schwendimann for suggestions. This work has been supported in part by the Fonds National Suisse de la Recherche Scientifique.

Correspondence and requests for materials should be addressed to M.S. (e-mail: Michele.Saba@epfl.ch).

Hierarchical self-assembly of metal nanostructures on diblock copolymer scaffolds

Ward A. Lopes*† & Heinrich M. Jaeger*

* *James Franck Institute and Department of Physics, The University of Chicago, Chicago, Illinois 60637, USA*

Self-assembly is emerging as an elegant, 'bottom-up' method for fabricating nanostructured materials[1–8]. This approach becomes particularly powerful when the ease and control offered by the self-assembly of organic components is combined with the electronic, magnetic or photonic properties of inorganic components[2,5,9]. Here we demonstrate a versatile hierarchical approach for the assembly of organic–inorganic, copolymer–metal nanostructures in which one level of self-assembly guides the next. In a first step, ultrathin diblock copolymer films form a regular scaffold of highly anisotropic, stripe-like domains[10–12]. During a second assembly step, differential wetting guides diffusing metal atoms to aggregate selectively along the scaffold, producing highly organized metal nanostructures. We find that, in contrast to the usual requirement of near-equilibrium conditions for ordering[2,3,13], the metal arranged on the copolymer scaffold produces the most highly ordered configurations when the system is far from equilibrium. We delineate two distinct assembly modes of the metal component—chains of separate nanoparticles and continuous wires—each characterized by different ordering kinetics and strikingly different current–voltage characteristics. These results therefore demonstrate the possibility of guided, large-scale assembly of laterally nanostructured systems.

Two important, competing, issues for the assembly of inorganic materials on organic scaffolds are high density and selectivity. In the case of scaffolds formed by copolymer domains (Fig. 1), preferential wetting of one of the copolymer blocks by metal will selectively aggregate the metal inside the corresponding domain[14,15]. However, simple coalescence of dense metal nanoparticle aggregates into the overall shape given by the boundaries of the selected copolymer domain—similar to that observed for water droplets filling out a narrow hydrophilic strip[3]—has not been achieved so far. This is because of the large surface energies of metals, exceeding those of copolymers by orders of magnitude. Consequently, metal–metal bonds will overwhelm metal–polymer bonds and, except for very small metal concentrations, the final configuration will be a large, spherical metal aggregate that completely ignores the polymer scaffold and mitigates selectivity. Thus, under equilibrium conditions even highly elongated, anisotropic polymer scaffolds may not be able to guide self-assembling metal particles into wire-like nanostructures. But here we show how non-equilibrium processes can induce, and stabilize, recognition of complex patterns provided by a nanoscale scaffold.

The particular, asymmetric polystyrene-block-poly(methylmethacrylate) (PS-b-PMMA) diblock copolymer that we used forms parallel cylindrical domains of PMMA, with a repeat spacing of 50 nm, surrounded by PS. Sample fabrication followed a two-level self-assembly process. First, spin-casting of the copolymer from solution to a thickness equivalent to one repeat spacing, and subsequent annealing, produced a thin film consisting of laterally alternating domains[11,12] (Fig. 1). Control over the domain curvature and orientation is possible, for example by applied in-plane electric fields[10,16], but was not the focus of the work described here. Instead, we consider the copolymer domain pattern as a given scaffold, and focus on the second assembly step, in which a small amount of metal (of nominal thickness 0.5–12 nm) was thermally evaporated onto the copolymer film, and the metal atoms were allowed to diffuse[17,18]. During this second step, the template morphology does not change as long as the molecular mass is sufficiently high that the order–disorder temperature is not reached[10].

For a wide range of metals and small deposited amounts (film thickness typically < 0.6 nm, depending on the metal and the deposition rate), selective decoration of one of the two copolymer domains is already apparent immediately after metal deposition (Fig. 2a). We observed this behaviour for Au, Ag, In, Pb, Sn and Bi, with Au and Ag preferring the PS domain, and In, Pb, Sn and Bi the PMMA domain. In each of these cases, the preferred domain becomes the scaffold. Selectivity of nearly 100% is achieved by warming the system in an inert gas atmosphere to a temperature that is above the copolymer glass temperature, but below the point at which the template pattern disintegrates (< 300 °C for PS-b-PMMA) (Fig. 2b). Inside the preferred domain, this leads to a coarsening that increases both the size and the separation of the nanoparticles while the metal also diffuses into the domains, perpendicular to the film plane[18,19]. With the exception of Ag, depositing larger amounts of metal does not fill out the domains. Rather than coalescing into continuous, elongated structures of high aspect ratio, the material ignores the template and 'jumps the

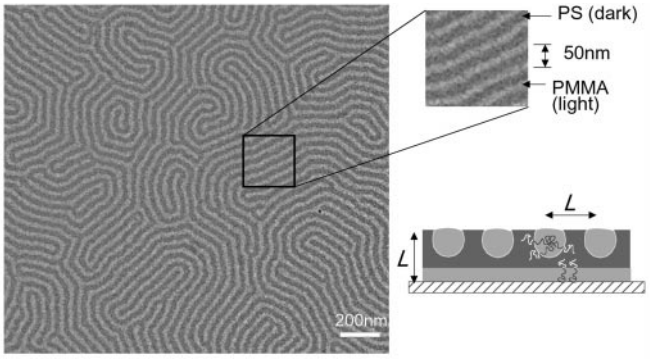

Figure 1 Transmission electron microscopy (TEM) image of ultrathin diblock copolymer film. The PS-b-PMMA copolymer (total molecular mass, 84,000; PS molecular mass, 60,000; polydispersity, 1.08; Soxhlet-extracted with cyclohexane to remove excess homopolymer PS in the diblock copolymer as obtained from Polysciences, Inc.) was spin-cast from solution to obtain a film thickness corresponding to the bulk repeat spacing, *L*. Spin-casting onto amorphous Si_3N_4 membrane substrates[25] allowed direct investigation by TEM without sample removal. The sketch shows a cross-section of the resulting film morphology. The striped domain pattern spontaneously forms as a consequence of phase separation between the two copolymer blocks, and provides the first level in a hierarchy of self-assembly levels. Image contrast results from electron-beam irradiation-thinning of the PMMA domains, which therefore appear lighter.

† Present address: Arryx Inc., 316 N. Michigan Avenue, Suite CL20, Chicago, Illinois 60601, USA.

© 2001 Macmillan Magazines Ltd